Title
A 200-GHz Inductively Tuned VCO with $-$7-dBm Output Power in 130-nm SiGe BiCMOS

Journal
IEEE Transactions on Microwave Theory and Techniques, 61(10)

ISSN
0018-9480

Authors
Chiang, PY
Momeni, O
Heydari, P

Publication Date
2013-09-23

DOI
10.1109/TMTT.2013.2279779

Peer reviewed

A 200-GHz Inductively Tuned VCO With −7-dBm Output Power in 130-nm SiGe BiCMOS

Pei-Yuan Chiang, *Student Member, IEEE*, Omeed Momeni, *Member, IEEE*, and Payam Heydari, *Senior Member, IEEE*

***Abstract*—A highly efficient push–push voltage-controlled oscillator (VCO) with a new inductive frequency tuning topology for (sub) terahertz frequencies is presented. The tuning technique is based on a variable inductance seen at the emitter node of a base-degenerated transistor. The variable inductor exhibits high quality factor and high tuning range due to the tunable transistor transconductance via bias current. Fabricated in a 0.13-μm SiGe BiCMOS process, the VCO achieves a tuning range of 3.5% and an output power of −7.2 dBm at 201.5 GHz. The dc power consumption of the VCO is 30 mW, resulting in a high dc to RF power efficiency of 0.6% and a figure of merit (FoM_T) of −165, which is the highest FoM for any silicon-based VCO reported to date at this frequency range. To demonstrate the functionality of the tuning technique, three VCO prototypes at different oscillation frequencies, including one operating in the 222.7–229-GHz range, are implemented and measured.**

***Index Terms*—Clapp oscillator, Colpitts oscillator, inductive tuning, push–push oscillator, submillimeter wave, terahertz (THz), varactor-less tuning, voltage-controlled oscillator (VCO).**

I. Introduction

HIGH-FREQUENCY range including (sub) terahertz (THz) and millimeter-wave (mm-wave) presents a great promise for noninvasive active and passive imaging, chemical, and biological spectroscopy, multigigabit wireless communications, and short-range radars [1]–[5]. Towards realization of a high-performance (sub) THz system, one of the most challenging steps is to design a high-power, tunable, and efficient signal source [6]–[8]. A traditional way of designing a solid-state high-frequency signal source is to have a tunable low-frequency signal source, followed by a chain of Schottky diode multipliers and amplifiers in compound semiconductors [9]. Despite their limited cutoff frequency and breakdown voltage, recent advances in silicon-based technologies have made them potential candidates for implementation of highly integrated THz radiators and detectors. Recently, high-power and high-frequency oscillators have been demonstrated in silicon [10], [11]. However, having a power-efficient tunable signal source is necessary for many practical applications. A conventional and widely used way of controlling the oscillation frequency is to implement varactors in an LC oscillator [12], [13]. Nevertheless, a tight tradeoff exists between quality factor (Q-factor) and $C_{\max}/C_{\min}$ tuning ratio of varactors, which will be more stringent at higher frequencies. While the use of minimum-length varactors can improve the Q-factor, it decreases the tuning ratio due to parasitic capacitors. Furthermore, the varactors' loss varies significantly across the tuning range, resulting in dramatic variation in output power due to the limited negative resistance that transistors can provide at high frequency.

On the other hand, as oscillation frequency increases towards the THz band, the inductor size will decrease almost quadratically. This implies: 1) achieving Q-factors as high as 15–20 for small-size inductors (around 100 pH) is possible and 2) magnetic coupling with a coupling coefficient of 0.7 or more can be achieved. Therefore, inductive tuning VCOs can be considered as viable candidates for wider tuning range and higher and relatively constant output power across the band at mm-wave and THz frequencies. Varactor-less voltage-controlled oscillators (VCOs) using transformer coupling feedback have already been proposed for a wide-tuning-range and high-Q-factor LC tank [14]–[16]. The tuning range of this transformer-coupled inductance is determined by the mutual inductance M and the primary and secondary windings' current ratio which degrades at high frequency. Another varactor-less tuning topology is to introduce controllable phase delay along a ring oscillator [17].

In this paper, which is an extension of the work published in [18], an inductive tuning topology based on a variable inductance seen at the emitter of an RL-degenerated amplifier has been developed. This variable inductor exhibits a high quality factor and high tuning range due to the base-degenerated inductor and resistor. This inductor introduces a negative resistance that compensates fpr $1/g_m$ loss seen from the emitter node. Moreover, the base-degenerated resistor forms a tunable inductor controlled by the transistor's bias current. To verify the feasibility of this approach, multiple VCOs at different frequencies, including 198∼205 GHz, 209∼215 GHz, 218∼225 GHz, and 223∼229 GHz, are designed and implemented. The VCO, operating at 198∼205 GHz, can achieve an output power of $-7.2 \sim -7.75$ dBm and a dc power of 30 mW. The tuning range is 3.5% and the power efficiency is 0.6%. To the best of the authors' knowledge, this work presents the highest frequency inductively tuned oscillator with the highest power efficiency among silicon-based VCOs.

This paper is organized as follows. In Section II, the proposed inductive tuning circuit is introduced and analyzed. In

Manuscript received May 27, 2013; revised July 22, 2013; accepted July 25, 2013. Date of publication September 16, 2013; date of current version October 02, 2013. This work was supported in part by the National Science Foundation under Contract ECCS-1002294.

P.-Y. Chiang and P. Heydari are with the Nanoscale Communication IC (NCIC) Laboratory, University of California, Irvine, CA 92697 USA (e-mail: peiyuanc@uci.edu; payam@uci.edu).

O. Momeni is with the Department of Electrical and Computer Engineering, University of California, Davis, CA 95616 USA (e-mail: omomeni@ucdavis.edu).

Color versions of one or more of the figures in this paper are available online at http://ieeexplore.ieee.org.

Digital Object Identifier 10.1109/TMTT.2013.2279779

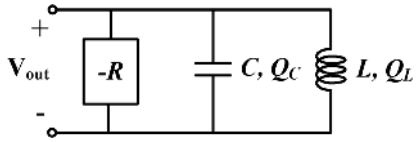

Fig. 1. *LC* tank with negative resistance.

Section III, test setup and measurement results of the 200-GHz inductively tuned push–push VCO are illustrated. In Section IV, we present the experimental results of the proposed tuning circuit, and Section V concludes the paper.

II. Inductive Tuning Circuit

Shown in Fig. 1 is an *LC* tank with a negative resistance cell where Q_C and Q_L represent the Q factor of the capacitor and the inductor, respectively. If the negative resistance cell, which is usually implemented using cross-coupled or Colpitts topologies, compensates for the loss of the *LC* tank, then the *LC* tank starts to oscillate. The oscillation frequency $\omega_{\rm osc}$ and Q factor of the tank $Q_{\rm tank}$ are expressed as [19]

$$\omega_{\rm osc} = \frac{1}{\sqrt{L(C+C_P)}} \quad Q_{\rm tank} = \frac{Q_C Q_L}{Q_C + Q_L} \tag{1}$$

where C_p denotes the parasitic capacitor of the negative resistor. The conventional varactor tuning is losing its advantages at high frequencies. The parasitic capacitors dominate the total capacitance and degrade the tuning range. Furthermore, low Q factor of varactors (i.e., only 2∼5 at 100 GHz) compared with Q_L of 20 decreases the Q factor of the *LC* tank, leading to smaller output power and higher phase noise. On the other hand, inductive tuning can be used to achieve higher $Q_{\rm tank}$ and tuning range, making it attractive for high-frequency VCO design.

A. Inductive Tuning Mechanism Using RL-Degenerated Transistor

It is commonly known that an emitter follower circuit with a small base resistor will generate an inductive reactance seen at the emitter node. Also, an inductor placed at the base terminal causes the emitter follower circuit to go to an unstable region due to the negative resistor at the emitter node. We investigate a series *RL* circuit to be employed as the degeneration network of an emitter follower circuit for frequency tuning. To illustrate the idea, we first look into a differential base-degenerated amplifier shown in Fig. 2(a). The circuit is comprised of transistors $T_3 - T_4$, the series RL network $R_{BB} - L_{BB}$, and a tail current I_E. The input impedance $Z_{\rm in}$ can be expressed as

$$Z_{\rm in} = \frac{R_{BB} + r_\pi + j\omega(L_{BB} + r_\pi C_\pi R_{BB}) - \omega^2 r_\pi C_\pi L_{BB}}{1 + g_{m_{3,4}} r_\pi + j\omega r_\pi C_\pi} \tag{2}$$

$$\cong \frac{(R_{BB} + r_\pi - \omega^2 r_\pi C_\pi L_{BB})(1 + j\omega/z_0)}{g_{m_{3,4}} r_\pi (1 + j\omega/p_0)} \tag{3}$$

$$= R_1 \| j\omega L_1 + R_2 \tag{4}$$

in which

$$z_0 = \frac{R_{BB} + r_\pi - \omega^2 r_\pi C_\pi L_{BB}}{L_{BB} + r_\pi C_\pi R_{BB}} \quad p_0 = \frac{g_{m_{3,4}}}{C_\pi} = \omega_T \tag{5}$$

$$R_2 = \frac{R_{BB}}{g_{m_{3,4}} r_\pi} + \frac{1}{g_{m_{3,4}}} - \frac{\omega^2 L_{BB}}{\omega_T}. \tag{6}$$

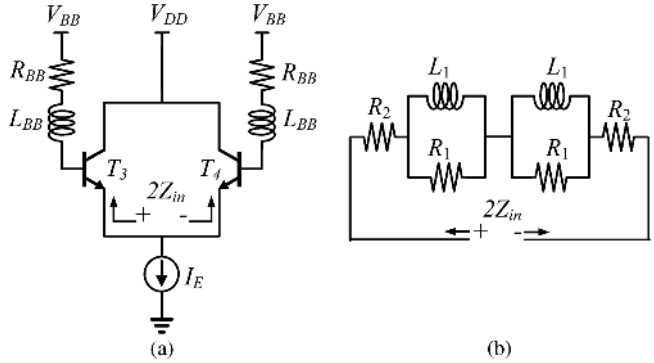

Fig. 2. (a) Differential RL-degenerated transistor pair and (b) its equivalent circuit.

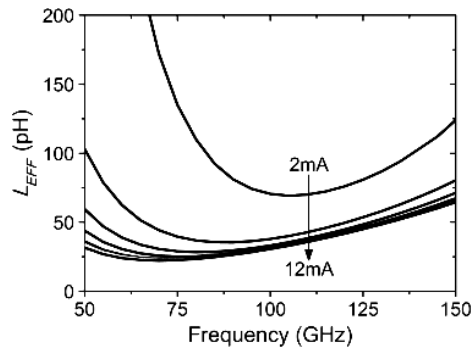

Fig. 3. Simulated $L_{\rm EFF}$ with respect to frequency for different values of I_E from 2 to 12 mA.

Assuming $g_{m3,4} r_\pi$, (2) is simplified to (3), which resembles the expression for the impedance of a network comprising a parallel $R_1 - L_1$ in series with R_2, as shown in Fig. 2(b). Substituting (5) and (6) into (2) results in the following closed-form expressions for R_1 and L_1:

$$R_1 = R_2 \left(\frac{p_0}{z_0} - 1 \right) = R_{BB} - \frac{1}{g_{m_{3,4}}} + \left(\left(\frac{\omega}{\omega_T} \right)^2 + \frac{1}{g_{m_{3,4}} r_\pi} \right) \omega_T L_{BB} \tag{7}$$

$$L_1 = \frac{R_1}{p_0} = \frac{R_{BB}}{\omega_T} - \frac{1}{g_{m_{3,4}} \omega_T} + \left(\left(\frac{\omega}{\omega_T} \right)^2 + \frac{1}{g_{m_{3,4}} r_\pi} \right) L_{BB}. \tag{8}$$

Substituting (6)–(8) into (4) yields a closed-form expression for driving point impedance seen from the emitter node of T_3, i.e.,

$$Z_{\rm in} \cong \frac{1}{g_{m_{3,4}}} - \frac{\omega^2 L_{BB}}{\omega_T} + \frac{\omega^2 R_{BB}}{\omega_T^2} + j\omega \left[\frac{R_{BB}}{\omega_T} - \frac{1}{g_{m_{3,4}} \omega_T} + \frac{\omega^2 L_{BB}}{\omega_T^2} \right] = R_{EFF} + j\omega L_{\rm EFF}. \tag{9}$$

R_2 in (6) is dominated by the last two terms, as R_{BB} (in the range of tens of ohms) is divided by the transistor's current gain $\beta_{3,4}$ (≥100). It will be equal to $1/g_{m3,4}$ if there is no L_{BB} and R_{BB}, as expected. L_{BB} contributes a negative term to both R_2 and $Z_{\rm in}$, thereby decreasing equivalent series loss of the variable inductor. R_{BB} is added to have inductance tuning ability via I_E. From (8), R_{BB} helps to boost variable inductance. From

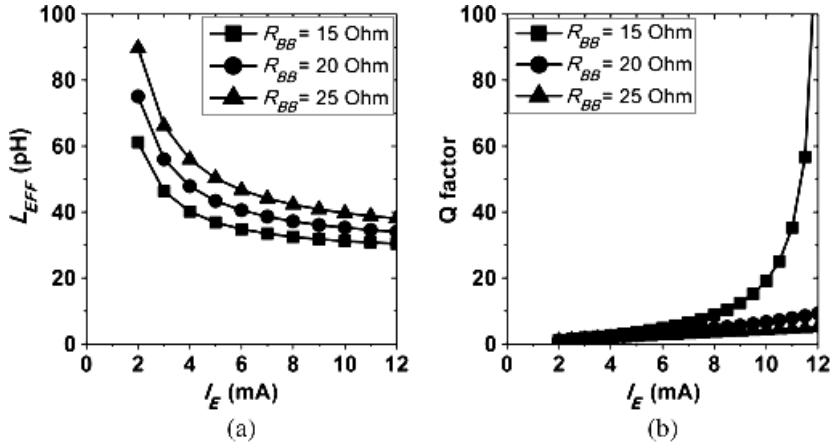

Fig. 4. (a) Simulated $L_{\rm EFF}$ versus I_E at 100 GHz for three different values of R_{BB}. (b) Corresponding quality factor.

(9), one can infer that the equivalent inductor $L_{\rm EFF}$ varies with I_E (through $g_{m3,4}$). Furthermore, $R_{\rm EFF}$ is reduced due to L_{BB}, and, thus, the quality factor is improved.

Fig. 3 shows the simulated $L_{\rm EFF}$ as a function of frequency with differential tail current I_E varying from 2 to 12 mA. In this simulation, the transistor size is 6 μm/0.13 μm, R_{BB} is 15 Ω, and L_{BB} is 60 H. From Fig. 3, as I_E increases from 2 to 12 mA $L_{\rm EFF}$ decreases from 70 to 30 pH around the 100-GHz fundamental frequency.

A tradeoff exists between the tuning range and quality factor of $L_{\rm EFF}$, as both $L_{\rm EFF}$ and $R_{\rm EFF}$ are directly affected by R_{BB}. Shown in Fig. 4(a) is $L_{\rm EFF}$ versus I_E at 100 GHz with three different values of R_{BB}, where L_{BB} is set to 60 pH. The simulated $L_{\rm EFF}$ increases with R_{BB}, while $L_{\rm EFF} - I_E$ variation follows the same behavior for all three values of R_{BB}. Fig. 4(b) depicts simulated Q factor of $L_{\rm EFF}$ with respect to I_E and shows that higher values of R_{BB} results in lower Q factor. Fig. 5 shows the simulated Q factor at 100 GHz versus I_E for three different values of L_{BB}, where R_{BB} is fixed at 15 Ω. In the low-I_E region, the Q factor is low because the transistors are not fully biased in forward active region. Once the transistors are biased in forward active region, the Q factor will increase. The Q factor will be boosted from 5 to 25 at $I_E = $ 10 mA when L_{BB} increases from 50 to 60 pH. This notion is also verified in (9).

Note that, if L_{BB} is chosen to be too large, it may cause an undesired oscillation due to the fact that the negative part of $R_{\rm EFF}$ will start dominating the other terms.

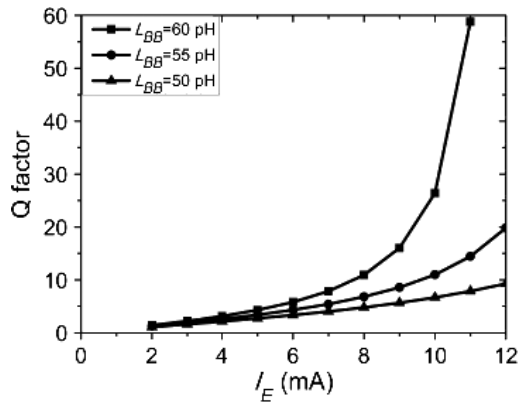

Fig. 5. The simulated Q factor of L_{EFF} at 100 GHz for three values of L_{BB}.

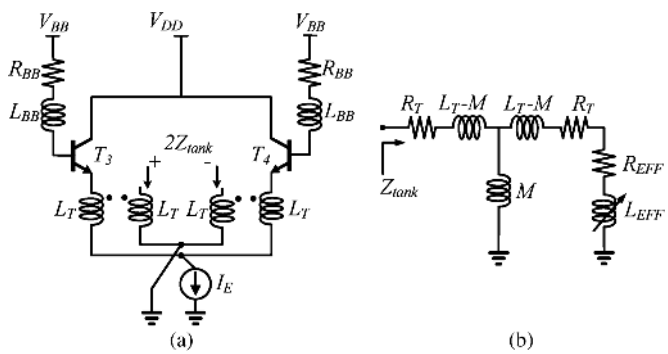

Fig. 6. (a) Proposed transformer coupled inductive tuning circuit and (b) it's half equivalent circuit.

B. Transformer-Coupled Inductive Tuning Circuit

The proposed inductive tuning circuit is shown in Fig. 6(a), where a 1:1 differential L_T transformer with coupling factor k_C is used to couple $L_{\rm EFF}$ to the oscillator's tank. The transformer isolates the dc bias current of the core oscillator from I_E, which is varying to achieve inductive tuning. A separate constant dc bias current is necessary for a VCO core because it provides constant negative resistance even in lower current tuning region. Furthermore, transformer coupling decreases the variation of Q factor. As shown in Fig. 5, the Q factor variation with a constant L_{BB} can be as high as 55. Such variation may lead to significant change in VCO output power, or it may even dampen the oscillation in the low Q region. To address this, the half equivalent circuit of the differential transformer coupled inductive tuning circuit in Fig. 6(a) is shown in Fig. 6(b). A T model [20] is used to represent the 1:1 transformer in Fig. 6(a). R_T represents the series loss of primary and secondary inductors and M denotes the mutual inductance. Assuming Q^2 of both the transformer and $L_{\rm EFF}$ to be much larger than 1, $Z_{\rm tank}$ can be expressed as

$$Z_{\rm tank} \cong R_T + \frac{(R_T + R_{\rm EFF})M^2}{(L_T + L_{\rm EFF})^2} + j\omega\left(\frac{L_T L_{\rm EFF} + L_T^2 - M^2}{L_T + L_{\rm EFF}}\right). \quad (10)$$

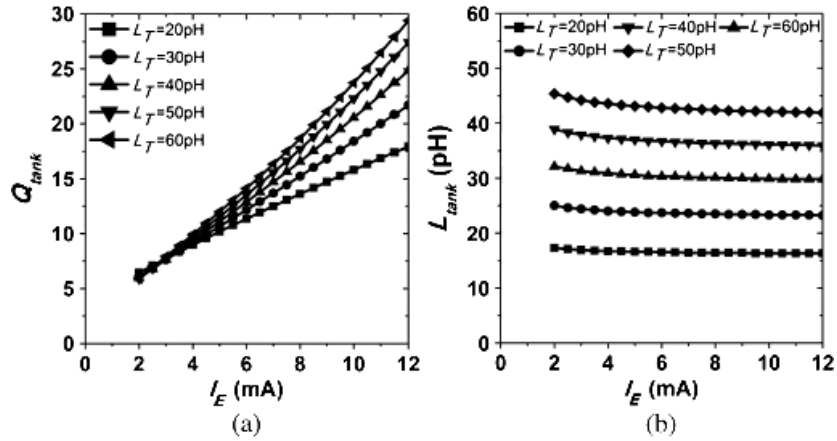

Fig. 7. (a) Simulated quality factor $Q_{\rm tank}$ of $Z_{\rm tank}$. (b) Inductor $L_{\rm tank}$ of $Z_{\rm tank}$ at 100 GHz, where L_{BB} is 60 pH, R_{BB} is 15 Ω, and the coupling factor k_C is 0.7.

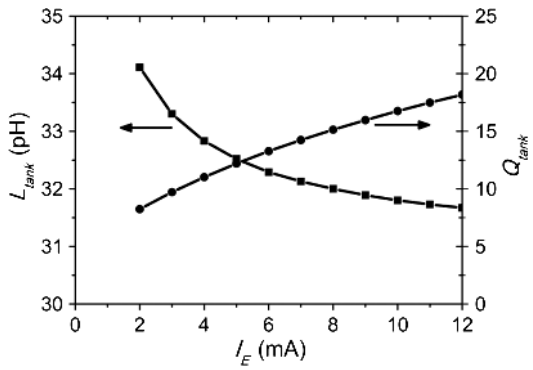

Fig. 8. Simulated inductance and Q factor of $L_{\rm tank}$ at 100 GHz, where L_T = 30 pH, $k_C = 0.7$, L_{BB} = 60 pH, and R_{BB} = 15 Ω.

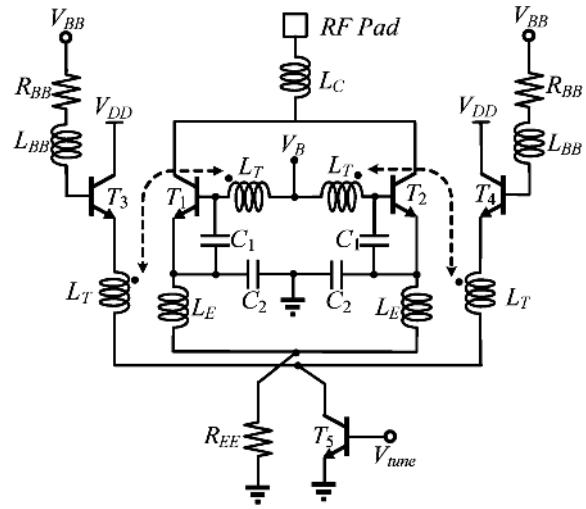

T_1~T_5	C_1	C_2	R_{BB}	R_E	L_T	L_E	L_{BB}
L_E=2×3μm	25fF	86fF	15Ω	38Ω	30pH	55pH	60pH

Fig. 9. Proposed inductively tuned push–push 200-GHz VCO.

Since, according to (10), $Z_{\rm tank}$ will retain higher percentage of the tuning range contributed by $L_{\rm EFF}$ as the transformer coupling increases, the transformer is designed to achieve a k_C factor of 0.7 and a Q factor of 15. Shown in Fig. 7(a) is the simulated Q factor of $Z_{\rm tank}$, $Q_{\rm tank}$, with five L_T values, where L_{BB} and R_{BB} are set to be 50 pH and 15 Ω, respectively. At the low I_E region, $Q_{\rm tank}$ is 6, which is higher than that of $L_{\rm EFF}$ in Fig. 5. As I_E increases, $Q_{\rm tank}$ will increase due to a decrease in $R_{\rm EFF}$. Moreover, higher L_T leads to additional improvement in $Q_{\rm tank}$, for a given I_E. As also shown in Fig. 7(b), for L_T varying from 20 to 60 pH, the tuning range slightly increases from 7% to 9%, while the average value of $L_{\rm tank}$ also increases from 18 to 45 pH. Therefore, the L_T transformer has to be designed based on the desired oscillation frequency with maximum achievable coupling factor. For the VCO in this work, L_T = 30 pH, L_{BB} = 60 pH and $R_{BB} = 15$ Ω, and the simulated $L_{\rm tank}$ and $Q_{\rm tank}$ versus I_E are shown in Fig. 8. The VCO with the proposed inductive tuning topology achieves an overall Q factor three times as high as the varactors' at 100 GHz. This Q factor will further increase towards the higher end of the tuning range. This helps the flatness of the VCO output power across the tuning range, because the higher Q factor at higher oscillation frequency compensates for degradation of the transistors' transconductance with frequency.

III. Inductively Tuned Push–Push VCO

Colpitts topology has proved to achieve a higher maximum oscillation frequency than a cross-coupled pair counterpart [21], [22], due to a nonunity-gain feedback loop realized using the tapped capacitor resonator, which decreases the capacitance contribution of C_π into the LC tank. Moreover, the phase noise of a Colpitts oscillator is a function of capacitive division ratio [22], making it more flexible to achieve a lower phase noise. Shown in Fig. 9 is the proposed schematic of the Colpitts push–push inductively tuned VCO. Owing to the core circuit comprising the transistor $T_1(T_2)$ and tapped capacitor network $C_1 - C_2$, a negative resistance can be seen at the base or collector nodes due to a capacitive feedback around these two nodes. The tank inductor L_T is placed at the base of $T_1(T_2)$, whose loss is compensated by the negative resistance. The oscillation frequency will be $1/[L_T C_1 C_2/(C_1 + C_2)]^{1/2}$. Together with the inductive tuning circuit composed of R_{BB}, L_{BB}, and $T_3(T_4)$, the oscillation frequency can be tuned by changing $V_{\rm tune}$. Note that, once oscillating, the second-harmonic signal

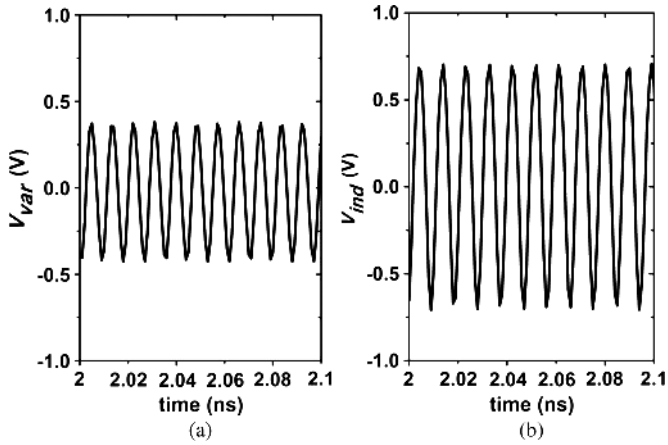

Fig. 10. Simulated voltage swing of the fundamental signal at the base node of a Colpitts VCO core for (a) conventional varactor-tuning VCO and (b) the proposed inductive-tuning VCO.

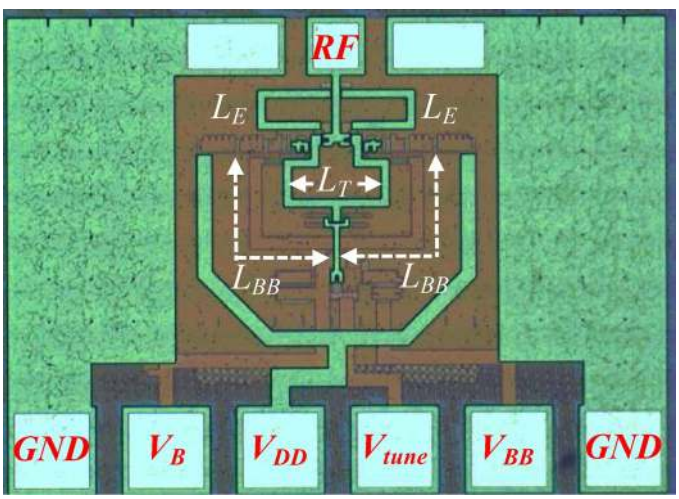

Fig. 11. Die photograph of the inductively tuned VCO where the chip area is $250\times290\ \mu m^2$ excluding the pad ring.

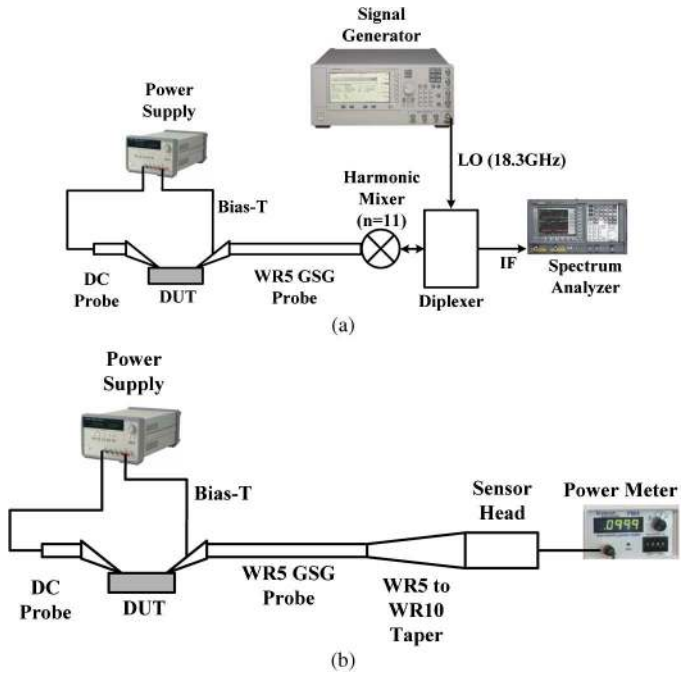

Fig. 12. (a). The 200-GHz VCO oscillation frequency measurement setup. (b). The 200-GHz VCO output power measurement setup.

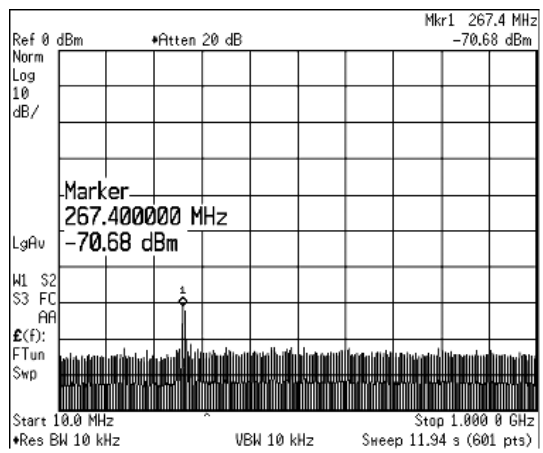

Fig. 13. IF tone shown on the spectrum analyzer after the VCO's 201.6-GHz output signal was down-converted by a harmonic mixer ($n = 11$) and LO frequency of 18.3 GHz.

can be extracted at any common-mode node of the VCO. In Fig. 9, the second harmonic is extracted from collectors in order to achieve higher output power. The primary reason is that the major portion of the second-harmonic current generated by transistors $T_1 - T_2$ will flow out from their collector nodes to the output load, while, for the other common-mode nodes, the inherent current division will degrade the output power. Also, placing the tank inductor at the base node eliminates the passive loss in the second signal path which would otherwise exist if that inductor would have been placed at collector node. The resistor R_{EE} is used to improve common mode rejection. However, there is a tradeoff between the second-harmonic output power and R_{EE} value to improve common-mode rejection, as R_{EE} is also in the second-harmonic path.

The inductor L_C in Fig. 9 models the wiring interconnection from collectors to RF pads and is considered to be part of the output-matching network along with the RF pad's parasitic capacitor. The common-mode node between C_2's is grounded to improve output matching at the second harmonic. With a bias-T implemented on a ground–signal–ground (GSG) waveguide probe, the dc supply voltage can be applied directly into the circuit, while the signal can be brought out from this probe to measurement equipment.

As illustrated in Section II, the Q factor of the proposed inductive-tuning LC tank is higher than that of the conventional varactor-tuning LC tank. A varactor-tuning VCO with the same oscillation frequency and tuning range is designed for comparison. The base voltage swing of the fundamental signal for transistor $T_1(T_2)$ is simulated and shown in Fig. 10, where the voltage swing of the inductive-tuning VCO is higher than the conventional one. This higher voltage swing means that: 1) the Q factor of the LC tank is higher as long as the swing does not exceed saturation region; 2) transistors $T_1 - T_2$ can generate a stronger second-harmonic signal; and 3) phase noise is improved due to

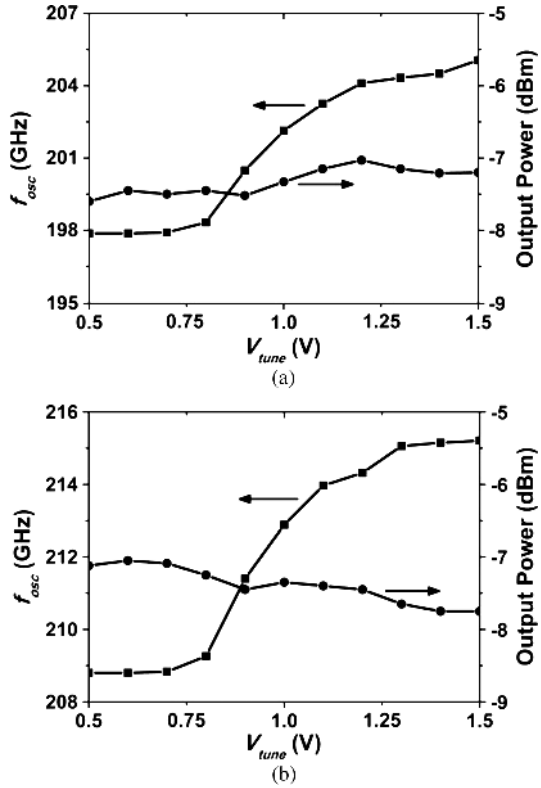

Fig. 14. Measured oscillation frequency and output power versus $V_{\rm tune}$ of (a) 200-GHz VCO and (b) 210-GHz VCO.

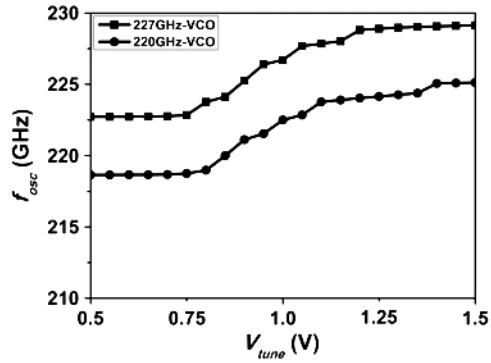

Fig. 15. Measured oscillation frequency of the 220- and 227-GHz VCOs.

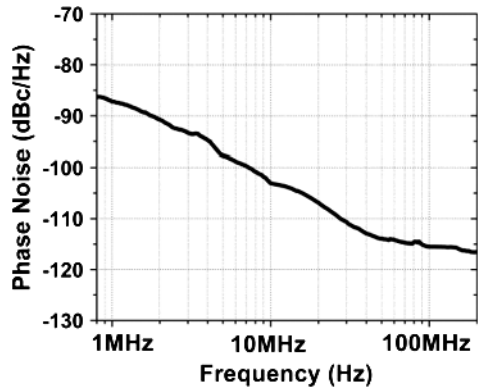

Fig. 16. Measured phase noise of the 200-GHz VCO.

the fact that it is proportional to $1/Q_{\rm tank}$ [23]. In our simulation, the output power of the proposed inductive-tuning VCO is 3 dBm higher than that of the conventional counterpart.

IV. Measurement Setup and Experimental Results

The proposed inductive tuning VCO was designed and fabricated in a 0.13-μm SiGe BiCMOS technology. All of the transformers and inductors were implemented on the two topmost metal layers, M5-M6, with the bottom metal layer M1 being used as a ground plain, shielding from the lossy substrate. Fig. 11 shows the chip photograph of the VCO with a chip area of 250×290 μm^2 excluding the pad ring. All of the elements and routing lines have been placed symmetrically in order to minimize mismatch and improve overall performance.

The 200-GHz VCO frequency and power measurement setups were configured as shown in Fig. 12(a) and (b). For frequency measurement, the VCO output signal was brought through the RF probe to a harmonic mixer, then down-converted to around 5 GHz, and measured on a spectrum analyzer. In Fig. 12(a), a GGB WR5 GSG probe with bias tee, an Agilent E4407 spectrum analyzer, a Pacific Millimeter GM harmonic mixer and MD4A diplexer are used to verify the oscillation frequency. Fig. 13 shows the down-converted 201.6-GHz VCO output signal when an LO signal of 18.3 GHz and a harmonic number of 11 is utilized. Due to the narrow IF bandwidth of the diplexer compared with the tuning range of the VCO, the LO frequency needs to be adjusted with respect to the VCO oscillation frequency. To accurately measure the output power, a direct power measurement setup was used, as shown in Fig. 12(b). The WR5 GSG probe is converted to a WR10 waveguide via a taper, and then connected to a power sensor and an Erickson PM4 power meter. The measured output power levels need to be calibrated by 3.25 dB to account for the loss of the probe, waveguide extension, and taper.

Fig. 14(a) shows the measured oscillation frequency and output power of the 200-GHz VCO with respect to the tuning voltage, $V_{\rm tune}$. By controlling $V_{\rm tune}$ from 0.5 to 1.5 V, the oscillation frequency is varied from 198 to 205 GHz, resulting in a tuning range of 3.5%. The measured output power is −7.2 dBm with less than 0.5-dB variation across the band. Fig. 14(b) shows the measured performance of a 212-GHz VCO prototype, which was designed using the same topology. The tuning range is from 209 to 215 GHz with −7.1-dBm output power. Both VCOs consume a dc power of 30–57 mW with respect to $V_{\rm tune}$. As shown in Fig. 15, two additional VCOs were implemented for 220 and 227 GHz. The measured tuning range is 6 GHz when the maximum oscillation frequency extends to 229 GHz. Due to the bandwidth limitation of WR5 waveguide (140–220 GHz), the output power of these two VCOs could not be measured accurately. Fig. 16 shows the measured phase-noise profile of the 200-GHz VCO, wherein the phase noises of −87.2 and −103.1 dBc/Hz are reported at 1- and 10-MHz offset, respectively. Table I shows the performance comparison with prior work. The proposed VCOs show a maximum figure of merit (FoM) (FoM_T) of −165.6,

TABLE I
VCO PERFORMANCE COMPARISON

	This Work	This Work	[24]	[25]	[26]	[27]	[28]	[29]
Frequency (GHz)	201.5	212	161.1	184.2	277.6	196.5	139	290
Tuning Range	3.5%	2.8%	4.7%	2%	1.5%	1.5%	0.09%	4.5%
Power(dBm)	-7.2	-7.1	-15	-11	-20	-19	-19	-1.2*
DC Power (mW)	30 (min.)	30 (min.)	46.5	95	132	29	9.6	325
Power Efficiency	0.64%	0.65%	0.068%	0.084%	0.0076%	0.087%	0.13%	0.23%
PN @ 1MHz (dBc/Hz)	-87	-92	-86	NA	NA	-94	-79	-78
FOM$_T$**	-162	-165.6	-151.9	NA	NA	-150	-112.1	-154
Technology	0.13μm SiGe	0.13μm SiGe	0.25μm SiGe	0.13μm SiGe	0.13μm SiGe	90nm CMOS	90nm CMOS	65nm CMOS

* Power combination of four cross-coupled oscillators.

** $\mathrm{FoM}_T = PN - 20\log((f_o/\Delta f)\cdot(FTR/10)) + 10\log(P_{\mathrm{DISS}}/1\ \mathrm{mW}) - P_{\mathrm{out}}$

which was the highest compared with the state of the art in silicon-based VCOs.

V. CONCLUSION

A varactor-less push–push VCO topology has been presented and analyzed for mm-wave and THz frequency bands. Four VCOs with different frequencies have been implemented to show the feasibility of the proposed approach. The maximum tuning range is 3.5% and highest oscillation frequency is 229 GHz. A power efficiency of 0.65% was achieved with an output power of -7.2 dBm. The proposed inductive tuning topology increases the Q factor of the VCO LC tank, which improves the output power and phase noise, resulting in a higher FoM among the other silicon-based low-THz VCOs.

ACKNOWLEDGMENT

The authors would like to thank Prof. G. Rebeiz, University of California at San Diego, La Jolla, CA, USA, for providing access to the 200-GHz measurement facility and M. Uzunkol for help in measurement. The authors would also like to acknowledge TowerJazz Semiconductor for chip fabrication. Technical support from Sonnet Software is highly appreciated.

REFERENCES

[1] P. Siegel, "Terahertz technology," *IEEE Trans. Microw. Theory Tech.*, vol. 50, no. 3, pp. 910–928, Mar. 2002.

[2] Z. Taylor, R. Singh, D. Bennett, P. Tewari, C. Kealey, N. Bajwa, M. Culjat, A. Stojadinovic, H. Lee, J.-P. Hubschman, E. Brown, and W. Grundfest, "THz medical imaging: *In vivo* hydration sensing," *IEEE Trans. Terahertz Sci. Technol.*, vol. 1, no. 1, pp. 201–219, Sep. 2011.

[3] C. Kulesa, "Terahertz spectroscopy for astronomy: From comets to cosmology," *IEEE Trans. Terahertz Sci. Technol.*, vol. 1, no. 1, pp. 232–240, Sep. 2011.

[4] K. Ajito and Y. Ueno, "THz chemical imaging for biological applications," *IEEE Trans. Terahertz Sci. Technol.*, vol. 1, no. 1, pp. 293–300, Sep. 2011.

[5] Z. Wang, P.-Y. Chiang, P. Nazari, C.-C. Wang, Z. Chen, and P. Heydari, "A 210 GHz fully integrated differential transceiver with fundamental-frequency VCO in 32 nm SOI CMOS," in *IEEE ISSCC Dig. Tech. Papers*, Feb. 2013, pp. 136–137.

[6] K. Sengupta and A. Hajimiri, "Distributed active radiation for THz signal generation," in *IEEE ISSCC Dig. Tech. Papers*, Feb. 2011, pp. 288–289.

[7] Y. M. Tousi, O. Momeni, and E. Afshari, "A novel CMOS high-power terahertz VCO based on coupled oscillators: Theory and implementation," *IEEE J. Solid-State Circuits*, vol. 47, no. 12, pp. 3032–3042, Dec. 2012.

[8] J. Sharma and H. Krishnaswamy, "216- and 316-GHz 45-nm SOI CMOS signal sources based on a maximum-gain ring oscillator topology," *IEEE Trans. Microw. Theory Tech.*, vol. 61, no. 1, pp. 492–504, Jan 2013.

[9] T. W. Crow, W. L. Bishop, D. W. Porterfield, J. L. Hesler, and R. M. Weikle, "Opening the THz window with integrated diode circuits," *IEEE J. Solid-State Circuits*, vol. 40, no. 10, pp. 2104–2110, Oct. 2005.

[10] O. Momeni and E. Afshari, "High power terahertz and millimeter-wave oscillator design: A systematic approach," *IEEE J. Solid-State Circuits*, vol. 46, no. 3, pp. 583–297, Mar. 2011.

[11] B. Razavi, "A 300-GHz fundamental oscillator in 65-nm CMOS technology," *IEEE J. Solid-State Circuits*, vol. 46, no. 4, pp. 894–903, Apr. 2011.

[12] I. Shen and C. F. Jou, "An X-band capacitor-coupled QVCO using sinusoidal current bias technique," *IEEE Trans. Microw. Theory Tech.*, vol. 60, no. 2, pp. 318–328, Feb. 2012.

[13] Z. Chen, C.-C. Wang, and P. Heydari, "W-band frequency synthesis using a Ka-band PLL and two different frequency triplers," in *IEEE RFIC Symp. Dig.*, Jun. 2011, pp. 83–86.

[14] G. Cusmai, M. Repossi, G. Albasini, A. Mazzanti, and F. Svelto, "A magnetically tuned quadrature oscillator," *IEEE J. Solid-State Circuits*, vol. 42, no. 12, pp. 2870–2877, Dec. 2007.

[15] D. Pi, B.-K. Chun, and P. Heydari, "A 2.5–3.2 GHz CMOS differentially-controlled continuously-tuned varactor-less LC-VCO," in *Proc. IEEE ASSCC*, 2007, pp. 111–114.

[16] K. KaChun, J. R. Long, and J. J. Pekarik, "A 23-to-29 GHz differentially tuned varactorless VCO in 0.13 μm CMOS," in *IEEE ISSCC Dig.*, Feb. 2007, pp. 194–596.

[17] S. Rong and H. C. Luong, "Design and analysis of varactor-less interpolative-phase-tuning millimeter-wave LC oscillators with multiphase outputs," *IEEE J. Solid-State Circuits*, vol. 46, no. 8, pp. 1810–1819, Aug. 2011.

[18] P.-Y. Chiang, O. Momeni, and P. Heydari, "A highly efficient 0.2 THz varactor-less VCO with -7 dBm output power in 130 nm BiCMOS," in *Proc. IEEE Compound Semiconductor IC Symp.*, Oct. 2012, pp. 1–4.

[19] L. Li, P. Reynaert, and M. S. J. Steyaert, "Design and analysis of a 90 nm mm-wave oscillator using inductive-division LC tank," *IEEE J. Solid-State Circuits*, vol. 44, no. 7, pp. 1950–1958, Jul. 2009.

[20] J. Long, "Monolithic transformers for silicon RF IC design," *IEEE J. Solid-State Circuits*, vol. 35, no. 9, pp. 1368–1382, Sep. 2000.

[21] C.-C. Wang, Z. Chen, and P. Heydari, "W-band silicon-based frequency synthesizers using injection-locked and harmonic triplers," *IEEE Trans. Microw. Theory Tech.*, vol. 60, no. 5, pp. 1307–1320, May 2012.

[22] V. Jain, B. Javid, and P. Heydari, "A BiCMOS dual-band millimeter-wave frequency synthesizer for automotive radars," *IEEE J. Solid-State Circuits*, vol. 44, no. 8, pp. 2100–2113, Aug. 2009.

[23] A. Hajimiri and T. H. Lee, "A general theory of phase noise in electrical oscillators," *IEEE J. Solid-State Circuits*, vol. 33, no. 2, pp. 179–194, Feb. 1998.

[24] Y. Zhao, B. Heinemann, and U. R. Pfeiffer, "Fundamental mode colpitts VCOs at 115 and 165-GHz," in *Proc. IEEE Bipolar/BiCMOS Circuits Technol. Meeting*, 2011, pp. 33–36.

[25] H. Rücker, B. Heinemann, W. Winkler, R. Barth, J. Borngräber, J. Drews, G. G. Fischer, A. Fox, T. Grabolla, U. Haak, D. Knoll, F. Korndörfer, A. Mai, S. Marschmeyer, P. Schley, D. Schmidt, J. Schmidt, K. Schulz, B. Tillack, D. Wolansky, and Y. Yamamoto, "A 0.13 μm SiGe BiCMOS technology featuring $f_T/f_{\max}$ of 240/330 GHz and gate delays below 3 ps," *IEEE J. Solid-State Circuits*, vol. 45, no. 9, pp. 1678–1686, Sep. 2010.

[26] R. Wanner, R. Lachnert, G. R. Olbrich, and P. Russer, "A SiGe monolithically integrated 278 GHz push-push oscillator," in *2007 MTT-S Int. Microwave Symp. Dig.*, Jun. 2007, pp. 333–336.

[27] H. Y. Chang and H. Wang, "A 98/196 GHz low phase noise voltage controlled oscillator with a mode selector using a 90 nm CMOS process," *IEEE Microw. Wireless Compon. Lett.*, vol. 19, no. 3, pp. 170–172, Mar. 2009.

[28] E. Seok, D. Shim, C. Mao, R. Han, S. Sankaran, C. Cao, W. Knap, and K. K. O, "Progress and challenges towards terahertz CMOS integrated circuits," *IEEE J. Solid-State Circuits*, vol. 45, no. 8, pp. 1554–1564, Aug. 2010.

[29] Y. M. Tousi, O. Momeni, and E. Afshari, "A 283-to-296 GHz VCO with 0.76 mW peak output power in 65 nm CMOS," in *IEEE Int. Solid-State Circuits Conf. Dig. Tech. Papers*, Feb. 2011, pp. 286–288.

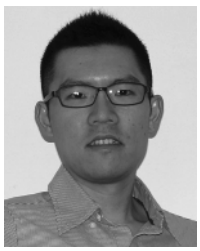

Pei-Yuan Chiang (S'12) received the B.S. and M.S. degrees in communication engineering from National Chiao Tung University, Hsinchu, Taiwan, in 2006 and 2008, respectively. He is currently working toward the Ph.D. degree in electrical engineering at the University of California, Irvine, CA, USA.

His research interests include millimeter-wave and terahertz integrated circuit design for wireless and high speed data communication. From June 2012 to December 2012, he was with Wireless/Bluetooth Group, Broadcom Corporation, Irvine, CA, USA, where he involved in the development of 60-GHz CMOS radio chips.

Omeed Momeni (S'04–M'12) received the B.Sc. degree from Isfahan University of Technology, Isfahan, Iran, in 2002, the M.S. degree from the University of Southern California, Los Angeles, CA, USA, in 2006, and the Ph.D. degree from Cornell University, Ithaca, NY, USA, in 2011, all in electrical engineering.

He joined the faculty of the Electrical and Computer Engineering Department, University of California, Davis, CA, USA, in 2011. He was a Visiting Professor with the Electrical Engineering and Computer Science Department, University of California, Irvine, CA, USA, from 2011 to 2012. From 2004 to 2006, he was with the National Aeronautics and Space Administration (NASA), Jet Propulsion Laboratory (JPL), to design L-band transceivers for synthetic aperture radars and high-power amplifiers for Mass Spectrometer applications. His research interests include millimeter-wave and terahertz integrated circuits and systems.

Prof. Momeni was the recipient of the Best Ph.D. Thesis Award from Cornell University's Electrical and Computer Engineering Department in 2011, the Outstanding Graduate Award from the Association of Professors and Scholars of Iranian Heritage (APSIH) in 2011, the Best Student Paper Award at the IEEE Workshop on Microwave Passive Circuits and Filters in 2010, the Cornell University Jacob's Fellowship in 2007, and the NASA-JPL Fellowship in 2003.

Payam Heydari (S'98–M'00–SM'07) received the B.S. and M.S. degrees (with highest honors) from the Sharif University of Technology, Tehran, Iran, in 1992 and 1995, respectively, and the Ph.D. degree from the University of Southern California, Los Angeles, CA, USA, in 2001, all in electrical engineering.

In August 2001, he joined the University of California, Irvine (UC-Irvine), CA, USA, where he is currently a Professor of electrical engineering. His research interests include the design of high-speed analog, radio-frequency, and mixed-signal integrated circuits. He is the author or coauthor of one book and 100 journal and conference papers.

Dr. Heydari currently serves on the Executive and Technical Program Committees of Compound Semiconductor IC Symposium (CSICS). He was a guest editor of the IEEE JOURNAL OF SOLID-STATE CIRCUITS and served as an associate editor for the IEEE TRANSACTIONS ON CIRCUITS AND SYSTEMS—I: REGULAR PAPERS from 2006 to 2008. He was a Technical Program Committee member of the IEEE Custom Integrated Circuits Conference (CICC). He was named by The Office of Technology Alliances at UC-Irvine one of ten outstanding innovators at the university. He was the corecipient of the 2009 Business Plan Competition First Place Prize Award and Best Concept Paper Award both from Paul Merage School of Business at UC-Irvine. He was the recipient of the 2010 Faculty of the Year Award from UC-Irvine's Engineering Student Council (ECS), the 2009 School of Engineering Fariborz Maseeh Best Faculty Research Award, the 2007 IEEE Circuits and Systems Society Guillemin-Cauer Award, the 2005 National Science Foundation CAREER Award, the 2005 IEEE Circuits and Systems Society Darlington Award, the 2005 UC-Irvine's School of Engineering Teaching Excellence Award, the Best Paper Award at the 2000 IEEE International Conference on Computer Design (ICCD), the 2000 Honorable Award from the Department of Electrical Engineering Systems at the University of Southern California, and the 2001 Technical Excellence Award in the area of Electrical Engineering from the Association of Professors and Scholars of Iranian Heritage (APSIH). He was recognized as the 2004 Outstanding Faculty at the UCI's EECS Department. His research on novel low-power multipurpose multi-antenna RF front-ends received the Low-Power Design Contest Award at the 2008 IEEE International Symposium on Low-Power Electronics and Design.